Geochemistry, geochronology, and tectonic implications of jarosite mineralization in the northern Franklin Mountains, Dona Ana County, New Mexico

Virgil W. Lueth, Philip C. Goodell, Matthew T. Heizler, and Lisa Peters
1998, pp. 309-315. https://doi.org/10.56577/FFC-49.309

in:

Las Cruces Country II, Mack, G. H.; Austin, G. S.; Barker, J. M.; [eds.], New Mexico Geological Society 49 th Annual Fall Field Conference Guidebook, 325 p. https://doi.org/10.56577/FFC-49

This page is intentionally left blank to maintain order of facing pages.

GEOCHEMISTRY, GEOCHRONOLOGY, AND TECTONIC IMPLICATIONS OF JAROSITE MINERALIZATION IN THE NORTHERN FRANKLIN MOUNTAINS, DOÑA ANA COUNTY, NEW MEXICO

VIRGIL W. LUETH[1], PHILIP C. GOODELL[2], MATTHEW T. HEIZLER[1], and LISA PETERS[1]
[1]New Mexico Bureau of Mines and Mineral Resources, New Mexico Tech, 801 Leroy Place, Socorro, NM 87801;
[2]Department of Geological Sciences, University of Texas at El Paso, El Paso, TX 79968

Abstract—Hypogene jarosite, $K_2Fe_6(SO_4)_4(OH)_{12}$, has recently been identified at the Copiapo jarosite mine and Schneider claims in the Webb Gap area of the northern Franklin Mountains, south-central New Mexico. Coarse grain sizes, mineral paragenesis, and co-precipitation with barite, galena, and fluorite establish a hypogene origin. Jarosite at the Copiapo deposit is localized in an east-dipping, low-angle normal fault. Mineralization occurs in a paragenetic sequence of: (1) hydrated halloysite, (2) hematite-gypsum, (3) jarosite-fluorite, and (4) natrojarosite. Jarosite occurs in a quartz-breccia vein at the Schneider claims with fluorite-barite-galena. $^{40}Ar/^{39}Ar$ analyses yield geologically significant apparent ages of 4.68 ± 0.13 and 4.72 ± 0.28 Ma for jarosite and natrojarosite, respectively, from the Copiapo mine and are interpreted to indicate that mineralization occurred at 4.69 ± 0.12 Ma. An age of 3.25 ± 0.29 Ma was determined for jarosite from the Schneider claims that dates the age of galena-barite-fluorite mineralization. These ages partially constrain the age of faulting in the northern Franklin Mountains and slickensides in the jarosite orebody indicate more recent reactivation and rotation on the host faults.

INTRODUCTION

Webb Gap, located in the northern Franklin Mountains, Doña Ana County, New Mexico (Fig. 1), is host to an unusual type of mineralization. Jarosite, $K_2Fe_6(SO_4)_4(OH)_{12}$, occurs in abundance and is associated with hypogene barite-fluorite-galena mineralization. The material was mined for paint pigment in the 1920s by the F. Schneider Company of El Paso, Texas. The jarosite deposit at the Copiapo mine was described as "remarkable" by Dunham (1935), who first described the geologic character of the deposits in the area. Berliner (1949) provided a confidential report to the U.S. Bureau of Mines evaluating the economic potential of the Copiapo deposit. The first comprehensive geologic mapping of the area was done by Harbour (1972). A detailed map of the Anthony quadrangle that encompasses the north Franklin Mountains was produced by Kelley and Matheny (1983), and provides much of the geologic basis for this study. McLemore et al. (1996) sampled the deposits and reported on the metal contents of the ores. Detailed mapping of the mine area and workings were conducted in early 1996 by the authors. Initial reports on the geology, geochronology, and geochemistry of the deposits were done by Lueth and Goodell (1996) and Goodell et al. (1997).

Jarosite is most commonly recognized as a product of the weathering of pyrite. Recently, the mineral has been determined to be a product of reactions in volcanic steam-heated environments (Rye and Alpers, 1997). Jarosite is also known to precipitate from acid springs in muskegs (Michel and Van Everdingen, 1987) and from hypersaline acid springs (Macumber, 1992). Lueth and Heizler (1997) reported an occurrence of hypogene jarosite at the Hansonburg district. They suggested a hypogene origin for the jarosite associated with late-stage fluorite-barite-quartz mineralization. Jarosite has been identified as a late-stage mineral with fluorite and quartz at a number of other deposits in the Rio Grande rift (e.g., Tonuco Mountain, Potrillo Mountains, Gonzales mine) by the authors and is subject to continuing study. Jarosite is also present with fluorite at the south end of the Organ Mountains in the Bishop Cap hills, immediately north of the Franklin Mountains. Jarosite has also been reported as a hypogene mineral in other deposits (Berzina et al., 1966; Keith, et al., 1979; John et al., 1991).

Supergene jarosite has recently been determined to yield geologically significant $^{40}Ar/^{39}Ar$ age dates (Vasconcelos et al., 1994). The coarse-grained nature of the jarosite and hypogene origin provide the first opportunity to directly date mineralization in the study area and demonstrates the usefulness of jarosite $^{40}Ar/^{39}Ar$ dating. This

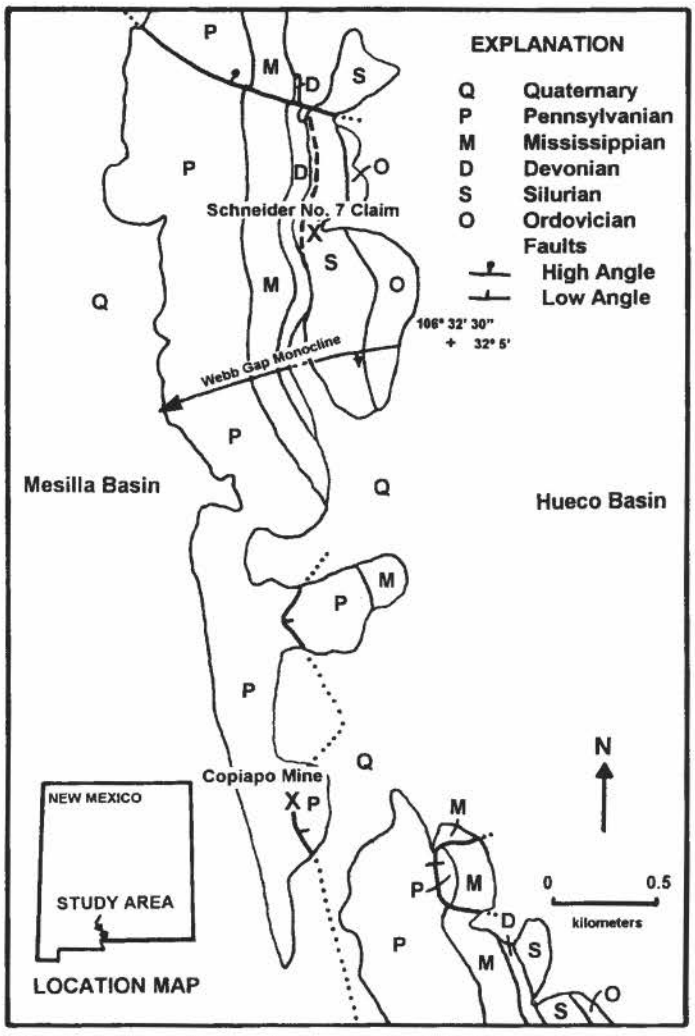

FIGURE 1. Generalized geologic map of the Webb Gap area. Map modified from Kelly and Matheny (1985).

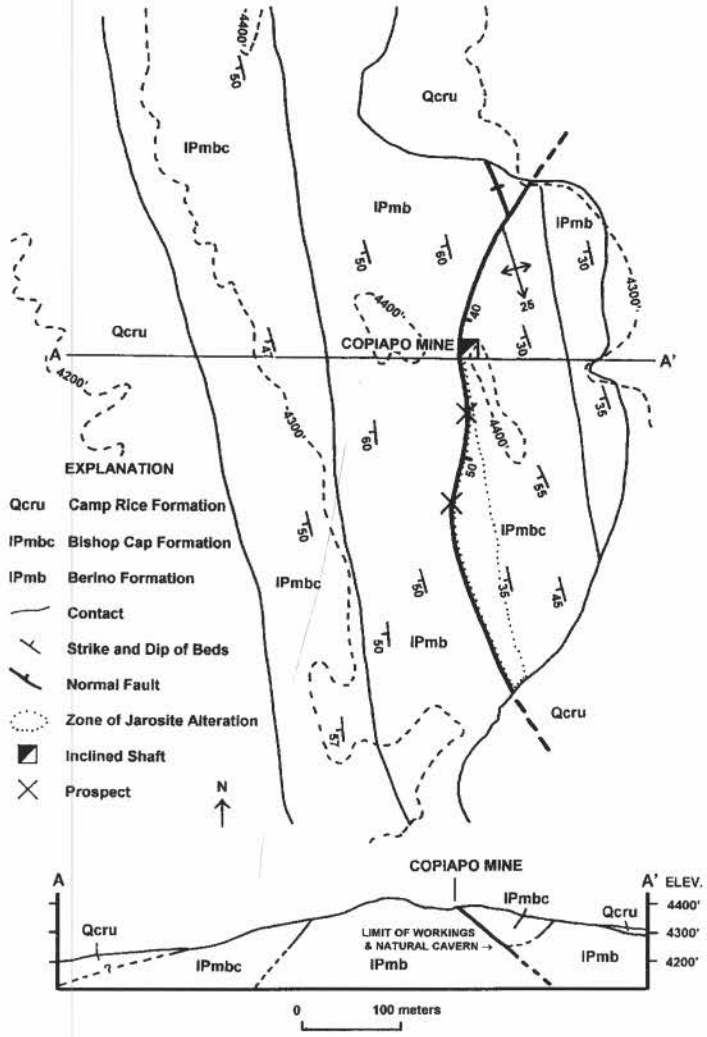

FIGURE 2. Geologic map and cross section of the Copiapo mine area.

study will describe the deposits, report ages for the jarosite, and discuss the geochemical and tectonic implications of the mineralization.

GEOLOGY OF THE WEBB GAP AREA

The Webb Gap area is a northern extension of the Franklin Mountains. These mountains are a tilted fault block, predominantly composed of west-dipping Paleozoic carbonate rocks that unconformably overlie Proterozoic granites and metamorphic rocks. In the study area, Ordovician through Pennsylvanian-age rocks are exposed (Fig. 1). Kelley and Matheny (1983) report two major episodes of structural deformation. The first is present as plunging fold structures and is considered to be a product of Laramide-age tectonism. The second major episode of deformation involves later dissection by low- and high-angle normal faults that were active during the Tertiary formation of the Rio Grande rift. The low-angle faults were interpreted by Kelley and Matheny (1983) to be initially high-angle normal faults that were rotated into shallower orientations by later fault development on the margins of the Mesilla and Hueco Basins.

MINERAL DEPOSITS

Copiapo mine

Mineralization at the Copiapo Jarosite mine occupies an east-dipping, low-angle (40–50°) normal fault, hereafter referred to as the Copiapo fault (Fig. 2). The footwall is formed by the Berino Formation (Pennsylvanian) with very little accompanying deformation and minor amounts of clay mineralization. The hanging wall consists of the Bishop Cap Limestone (Pennsylvanian) and is extensively deformed and mineralized. Drag folding, brecciation, and small scale faulting are present in the hanging wall block and are responsible for the shallow dips mapped near the mine area (Fig. 2). Post-mineralization faulting, evidenced by numerous slickensides and drag folding, are evident within the jarosite ore. Slickensides in the ore have rakes in the plane of the fault of less than 20° toward the south.

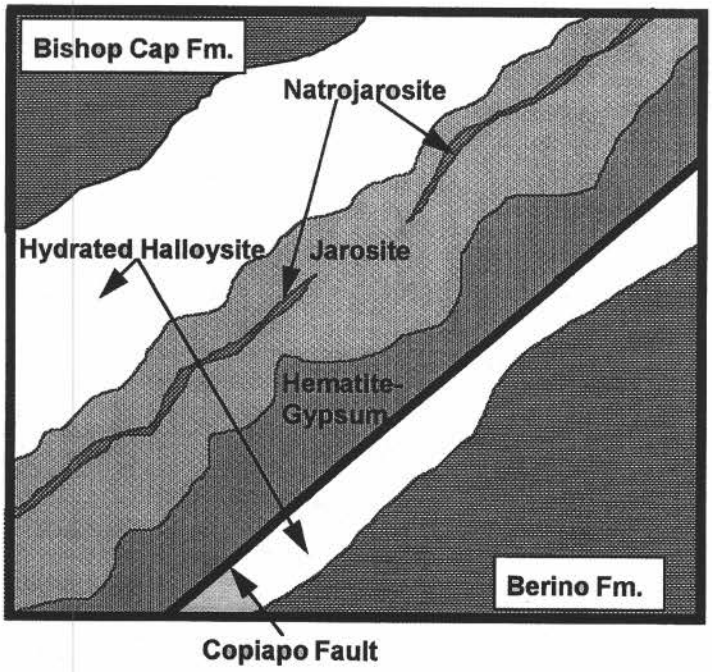

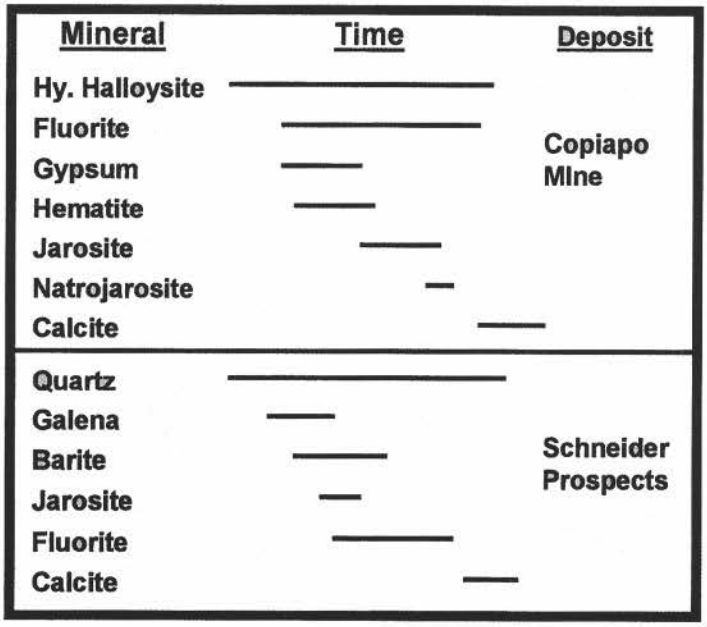

FIGURE 3. **A,** Schematic diagram of mineralization at the Copiapo mine, first level, south drift. Total thickness of mineralization depicted in the diagram is approximately 2 m. **B,** Paragenesis diagram illustrating the sequence of mineral precipitation based on textural relationships at the Copiapo and Schneider deposits.

The remarkable aspect of the mineralization at the Copiapo mine is the large volume and purity of jarosite. Recognizable jarosite mineralization at the surface extends over a north-south distance of 375 m with a maximum width of 40 m immediately south of the mine (Fig. 2). The deposit is developed by a 40° incline, parallel to the fault plane, to a depth of 60 m. Jarosite is exposed to a depth of 25 m down the incline. Maximum thickness of the ore observed in the first level of the mine is 2 m. The thickness of mineralization averages 1.2 m throughout the mine but is thickest near the surface and thins with depth. The ore was exploited on four levels, the 5th level at the bottom of the incline terminates at a north-south-trending cavern (Fig. 3) filled with calcite (variety onyx) flowstone. The 1st level is the most extensive with 75 m of workings as levels and stopes driven north and south of the incline. Levels 2, 3, and 4 each consist of 12 m of tunnels driven south of the incline. Levels 3 and 4 curve gently toward the southwest from the incline. The fifth level consists of 36 m of workings, not including natural openings. The cavern is developed in the hanging wall of the Copiapo fault at the contact between the Berino and Bishop Cap Formations. Extensive brecciation is present in the wall rocks along with recrystallization of the limestone and development of siderite.

The tabular body of mineralization consists of several mineralogical zones deposited in a definable paragenetic sequence (Fig. 4). Replacement textures are common in the ores. The first layer consists of hydrated halloysite, $Al_2Si_2O_5(OH)_4 \cdot 2H_2O$, in sharp contact with the fault plane and hanging-wall limestone. Hydrated halloysite completely surrounds jarosite and is present from the top to the bottom of the incline. Inside the hydrated halloysite is a layer of coarse-grained gypsum, variety selenite, and hematite. The hematite-gypsum layer is up to 0.3 m thick against the fault. In the hanging wall, the hematite-selenite layer is only 5 cm thick (Fig. 4). Pods of hematite occur in the jarosite layer and occasional pods of jarosite occur in the hematite-selenite. The texture of the hematite varies from ocherous to coarsely crystalline. The gypsum tends to be very coarse grained, attaining maximum crystal lengths of up to 8 cm. Locally, the gypsum is leached, leaving casts in the hematite. Coarsely crystalline zones of hematite-gypsum are chaotically distributed in the mine. In contrast, the contact between the hematite-gypsum layer and jarosite is sharp, often with sharp embayments of jarosite projecting into the hematite-gypsum layer. Direct replacement of hematite-gypsum by jarosite can be recognized by pseudomorphic textures of jarosite after hematite-gypsum. Grain sizes for jarosite vary from cryptocrystalline to grains up to 3 mm in diameter. Texture of the jarosite ranges from pulverulent to coarsely schistose and porous to massive. Within the jarosite layer, variations of color and grain size are common and chaotically distributed. The final layer in the paragenesis is a light yellow, pulverulent variety of natrojarosite $Na_2Fe_6(SO_4)_4(OH)_{12}$. Gash fractures within the jarosite and natrojarosite contain talcous, cryptocrystalline fluorite (confirmed by x-ray diffraction). X-ray analysis of jarosite samples also reveals a ubiquitous presence of fluorite disseminated throughout the jarosite ore. Fluorite was also detected by X-ray diffraction in the hydrated halloysite layers.

Schneider No. 7 claim

The Schneider No. 7 claim, is 1.6 km north of the Copiapo jarosite mine. The deposits of this area were initially described by Dunham (1935) as minor occurrences of barite, fluorite, and galena. No jarosite was reported. Mineralization is present in a 50°, east-dipping fault zone in the Fusselman Dolomite (Silurian). Bedded deposits are present as small manto-like bodies at the top of the Fusselman Dolomite, immediately beneath the contact with the Canutillo Formation (Devonian). Fracturing is most extensive

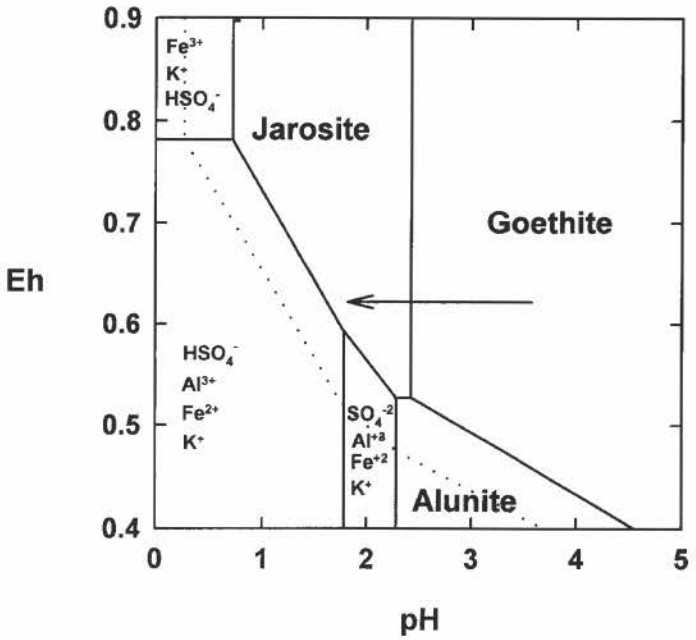

FIGURE 4. Eh-pH diagram depicting the stability fields of goethite-jarosite and aqueous species at 25° C and 101.3 kPa. Activities of species used in the calculations are: $(a_{\Sigma S}) = 10^{-2}$ m; $(a_{\Sigma Fe^{2+}}, {}_{Fe^{3+}}) = 10^{-1}$ m; $(a_{Al^{3+}}) = 10^{-3}$ m; $(a_{K^+}) = 10^{-3}$ m. Dashed lines represent $(a_{\Sigma Fe^{2+}}, {}_{Fe^{3+}}) = 10^{-3}$. Diagram modified from Keith et al. (1979). The arrow indicates a hypothetical decrease in pH that could lead to the formation of jarosite at the expense of goethite (hematite) and produce the assemblage observed at the Copiapo mine.

in the hanging wall of mineralization. Faulting connects the bedded deposits to a steeply dipping quartz-breccia zone. The quartz-breccia zone is within the plane of the fault but quartz mineralization is not uniformly distributed and the quartz-breccia body is more pipe-like in form. The quartz ore is cut by a number of secondary faults that strike N5°W and dip greater than 53°E. Subhorizontal slickensides are present on the fault surfaces, similar to those at the Copiapo mine. Significant amounts of hematite, as larger blocks in the breccia, are also present. Blocks of unaltered limestone are also seen as large horse blocks.

Manto mineralization consists of barite, fluorite, and galena. Minor brecciation occurs in the contact between ore and host rocks. The majority of the mineralization is confined to an inclined breccia zone with small mantos emanating from the breccia. Within the mantos, galena is euhedral and widespread in the barite. Fluorite occurs as cubic crystals in voids. Banded calcite, similar to the cave flowstones at Copiapo, is present at the base of some mantos.

Pyrite, galena, barite, fluorite, and jarosite are also present in the quartz breccia as coarse grains, but most commonly as brecciated clasts. The minerals tend to be randomly distributed in the quartz. The galena shows very little alteration and, when present, consists of thin rims of anglesite. Paragenetic relationships are difficult to determine in the quartz breccia because of extensive fracturing. However, fluorite and barite tend be euhedral to subhedral and represent the latest stage of ore mineralization. The jarosite masses are most commonly brecciated, although grain textures tend to be coarse, up to 1 mm. Jarosite is often in contact with fluorite and not observed in contact with sulfide minerals.

GEOCHEMISTRY

Mineralogic and geologic relationships observed at the two deposits indicate a hypogene origin for the jarosite. This interpre-

tation is, at the Copiapo mine, based on the presence of fluorite and the coarse-grained nature of the jarosite. It is further supported by the abundance of potassium in the deposit because there are no potassium-bearing rocks in the stratigraphic sequence above the deposit to provide supergene-derived potassium. The abundance of potassium at the Copiapo mine in itself appears to preclude a supergene origin. The hypogene relationships are even more apparent at the Schneider claims where coarse-grained jarosite occurs directly with galena-fluorite-barite mineralization.

The mineralogy and paragenesis of the deposits in the Webb Gap area reflect mineralization by acidic and oxidized solutions. Hydrated halloysite and jarosite are stable at values of less than pH 4 (Polyak and Güven, 1996) and pH 3 (Stoffregen, 1993), respectively. The paragenetic sequence of hydrated halloysite, hematite-selenite, and jarosite can be formed by decreasing pH over time (Fig. 5). Initial acidification could have occurred by reaction with pyrite in the Canutillo and Percha Formations (which underlies the study area and is exposed north of Webb Gap) or from the interaction of a H_2S-rich fluid/vapor and oxidized groundwater. Precipitation of iron oxyhydroxides (hematite precursors?) would further acidify the solutions. Finally, once pH is low enough and jarosite becomes a stable phase, the precipitation of jarosite itself drives pH values lower (Long et al., 1992). The variable grain size and chaotic textures within the jarosite ore may be the result of multiple episodes of dissolution and reprecipitation. Additionally, potassium activity decreases with time as indicted by the presence of natrojarosite late in the paragenesis (Alpers et al., 1989). Natrojarosite does not form in the presence of potassium in most natural systems, although a complete solid solution can be attained in laboratory experiments (Stoffregen, 1993).

The formation of an acidic and oxidized fluid, outside the sulfide weathering environment, requires two fluids: (1) a H_2S-dominated fluid or vapor carrying Pb, Ba, K, and F and (2) an oxidized fluid, presumably shallow groundwater (Stoffregen, 1993). H_2S would react with oxygenated groundwater and produce sulfuric acid in a manner similar to that described for sulfuric acid speleogenesis (Hill, 1995). The presence of the cave below the mineralized zone may be a product of this process. Another jarosite-iron oxide mineralized quartz zone has also been described by Kelley and Matheny (1983) near Anthony Gap, south of Webb Gap. A small cavern system is also present there. The sulfuric acid dissolves the limestone, and as it becomes neutralized, precipitates hydrated halloysite. The formation of hydrated halloysite insulates later acidic solutions from the limestone. The precipitation of quartz at the Schneider deposit would be an analogous situation. Leaching of aluminum and silica-rich rocks (e.g., the Canutillo and Percha Formations) in the subsurface or undissolved residue in the limestone provides the clay components for the hydrated halloysite. Between the Copiapo and Schneider deposits is a zone of strongly silicified and leached outcrop of Percha and Canutillo Formations. The Percha Shale also contains abundant pyrite in areas removed from silicification and could provide a ready source of iron, potassium, aluminum and sulfate in the subsurface. Fluorine, barium, lead, and sulfur are probably derived from the H_2S-rich basin fluid, which migrated up boundary faults adjacent to the deep basins due to thermal buoyancy. We can infer temperatures of brine fluid responsible for mineralization range from 125–210°C by comparison to similar fluorite-barite-galena deposits (Macer, 1978; Putnam, 1981), including those in which jarosite has been identified, e.g., Bishop Cap and Hansonburg (Lueth and Heizler, 1997). Stable isotope analysis of the deposits is currently underway to further characterize the geochemical evolution of this and other jarosite-bearing fluorite-barite-galena deposits.

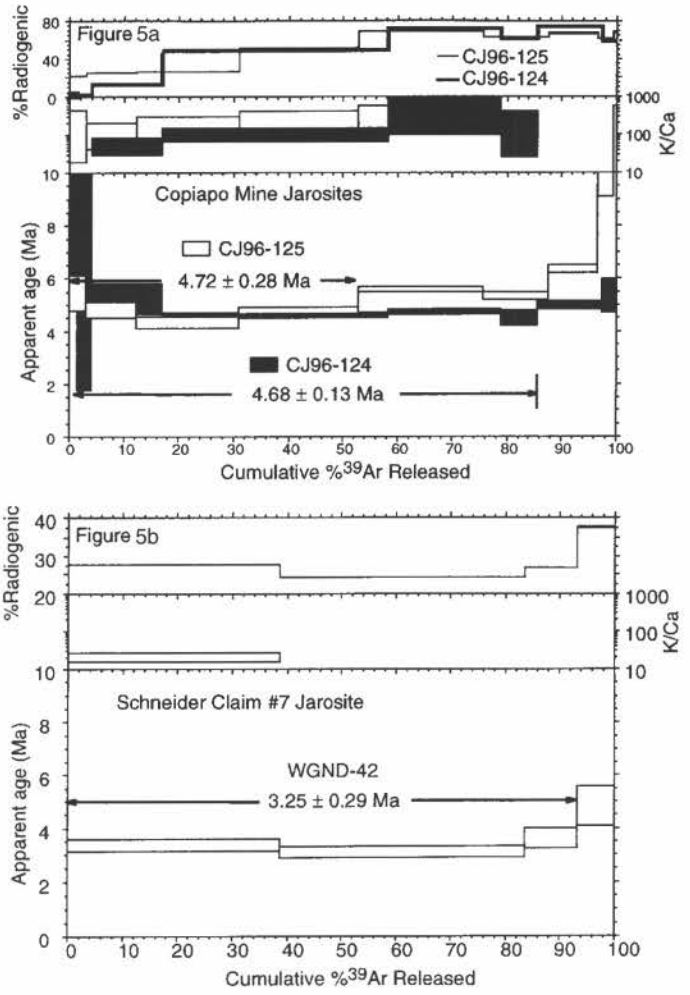

FIGURE 5. $^{40}Ar/^{39}Ar$ age spectra for: **A.** jarosite (CJ96-124) and natrojarosite (CJ96-125) from level 1 of the Copiapo mine, and **B.** jarosite from the Schneider deposit (WGNP-42).

$^{40}Ar/^{39}Ar$ GEOCHRONOLOGY

Methods and sample description

Hand-picked mineral separates of jarosite from the Copiapo and Schneider deposits were confirmed by X-ray diffraction at the New Mexico Bureau of Mines and Mineral Resources X-ray Lab. The x-ray patterns show that samples CJ96-124 and WGND-42 are apparently pure jarosite, whereas CJ96-125 is a natrojarosite. The samples were placed in machined aluminum discs along with interlaboratory standard Fish Canyon Tuff sanidine (age = 27.84 Ma; Deino and Potts, 1990) as a neutron flux monitor. The discs were sealed in an evacuated quartz tube and irradiated for 24 hrs in the L-67 position of the Ford Reactor at the Phoenix Memorial Laboratory, Ann Arbor, Michigan.

Following irradiation, samples and monitors were placed in an automated ultra-high vacuum extraction system. Individual crystals of monitor sanidine were placed in a copper planchet and fused with a 10W Synrad CO_2 continuous laser. Evolved gases were purified of reactive species for 2 min using a SAES GP-50 getter operated at ~450°C. J-factors were determined to a precision of ±0.1% (2σ) by analyzing four single crystal aliquots from each of the four radial positions around the irradiation vessel. Jarosite samples were step-heated in a double-vacuum Mo-resistance furnace. Evolved gases were purified during heating with a SAES GP-50 getter for 10 min, followed by an additional 8 min (for samples CJ96-124 and

TABLE 1. Analytical data from jarosites collected at the Copiapo and Schneider deposits.

ID	Temp (°C)	$^{40}Ar/^{39}Ar$	$^{37}Ar/^{39}Ar$	$^{36}Ar/^{39}Ar$ (x 10^{-3})	$^{39}Ar_K$ (x 10^{-15} mol)	K/Ca	^{40}Ar (%)	^{39}Ar (%)	Age (Ma)	±2σ (Ma)
CJ96-124 Jarosite, H:1:53, 4.92 mg, jarosite, 4.92 mg, J=0.00378453±0.10%, D-1.0074, nm-53, Lab#=6873-10										
A	*350*	*202.6*	*0.0000*	*674.0*	*2.20*	-	*1.7*	*1.4*	*23.0*	*18.2*
B	400	49.23	0.0000	163.2	4.22	-	2.0	4.0	6.7	4.9
C	425	5.984	0.0102	17.56	20.8	50.2	12.8	17.0	5.24	0.56
D	450	1.376	0.0052	2.273	66.2	98.9	49.2	58.2	4.62	0.10
E	475	0.9713	0.0008	0.8470	33.3	640.2	71.5	78.9	4.73	0.10
F	500	1.074	0.0047	1.299	10.4	107.9	61.8	85.4	4.52	0.29
G	*550*	*0.9875*	*0.0000*	*0.7627*	*19.2*	-	*74.4*	*97.3*	*5.01*	*0.17*
H	*600*	*1.350*	*0.0000*	*1.830*	*4.24*	-	*57.9*	*99.9*	*5.33*	*0.63*
I	*700*	*20.47*	*0.0000*	*21.59*	*0.070*	-	*68.7*	*100.0*	*93.6*	*35.2*
J	*750*	*36.49*	*0.0000*	*-22.9317*	*0.022*	-	*118.5*	*100.0*	*273.4*	*113.1*
total gas age			n=10		160.7	194.8			5.16	0.60
plateau			n=5	steps B–F	135.0	229.8		84.0	4.68	0.13
CJ96-125 Jarosite, F:10:53, 8.00 mg, Jarosite, 8.00 mg, J=0.00379419±0.10%, D=1.0074, nm-53, Lab#=6863-10										
A	350	3.728	0.0054	9.813	6.10	93.9	21.5	3.1	5.48	0.68
B	400	2.863	0.0056	7.210	18.5	91.7	24.7	12.3	4.83	0.31
C	425	2.409	0.0036	5.914	37.5	142.5	26.3	31.1	4.34	0.23
D	450	1.365	0.0026	2.154	43.2	194.5	51.4	52.7	4.80	0.13
E	475	1.190	0.0021	1.163	45.7	241.6	68.9	75.6	5.60	0.10
F	500	1.252	0.0000	1.492	23.9	-	62.6	87.5	5.36	0.14
G	550	1.393	0.0000	1.472	18.1	-	66.8	96.5	6.36	0.15
H	600	2.267	0.0000	2.836	5.63	-	61.8	99.4	9.57	0.45
I	700	13.71	0.0109	14.86	1.27	47.0	67.8	100.0	62.5	2.3
total gas age			n=9		199.8	135.8			5.63	0.20
plateau			n=9	steps A–I	199.8	135.8		100	5.5	1.2
WGND-42 Jarosite, H:4:53, 3.25 mg, jarosite, 3.25 mg, J=0.00378017±0.10%, D-1.0074, nm-53, Lab# =6875-01										
A	350	1.773	0.0249	4.252	25.0	20.5	27.7	38.5	3.35	0.22
B	400	1.859	0.0000	4.671	29.0	-	24.3	83.2	3.08	0.20
C	425	1.971	0.0000	4.791	6.31	-	26.8	92.9	3.60	0.39
D	*450*	*1.882*	*0.0000*	*3.886*	*4.40*	-	*37.5*	*99.7*	*4.81*	*0.74*
E	*475*	*-2.3718*	*0.0000*	*-20.7670*	*0.114*	-	*-157.*	*99.9*	*25.3*	*17.6*
F	*500*	*28.83*	*3.576*	*123.8*	*-0.014*	*0.14*	*-26.0*	*99.9*	*-51.9*	*116.0*
G	*550*	*55.58*	*7.940*	*156.9*	*0.020*	*0.064*	*17.6*	*99.9*	*66.0*	*85.5*
H	*600*	*52.05*	*16.81*	*390.3*	*0.067*	*0.030*	*-119.*	*100.0*	*-488.7*	*884.8*
total gas age			n=8		64.8	7.9			2.9	1.2
plateau			n=3	steps A–C	60.3	8.5		92.9	3.25	0.29

Isotopic ratios corrected for blank, radioactive decay, and mass discrimination, not corrected for interfering reactions.
Individual analyses show analytical error only; mean age errors also include error in J and irradiation parameters.
Analyses in italics are excluded from mean age calculations.
Correction factors:
$(^{39}Ar/^{37}Ar)_{Ca} = 0.00070 \pm 0.00005$
$(^{36}Ar/^{37}Ar)_{Ca} = 0.00026 \pm 0.00002$
$(^{36}Ar/^{39}Ar)_{K} = 0.0119$
$(^{40}Ar/^{39}Ar)_{K} = 0.0270 \pm 0.0020$

WGND-42) and 10 min (for sample CJ96-125) of cleanup using a separate SAES GP-50 getter. Argon isotopic compositions were determined with a MAP 215-50 mass spectrometer operated in static mode. Argon isotopes were detected by an electron multiplier with an overall sensitivity of about 1 x 10^{-16} moles/pA. Extraction system and mass spectrometer blanks and backgrounds were measured numerous times throughout the course of analysis. Typical furnace blanks were 2250, 6, 3, 8, 1.3 x 10^{-18} moles at atomic masses of 40, 39, 38, 37, and 36, respectively. Correction factors for interfering nuclear reactions were determined using K- and Ca-rich glasses and salts and are given in Table 1. Plateau ages for the age spectra are defined if three or more contiguous heating steps, which contain at least 50% of the total ^{39}Ar are deemed concordant at the 2σ confidence level (Fleck et al., 1977). The plateau ages are calculated by weighting the steps on the plateau by the inverse of their variance and the reported 2σ errors, which include the J-factor error, are calculated using the method of Samson and Alexander (1987). The decay constant and isotopic abundances used are those suggested by Steiger and Jager (1977).

Results and age spectra discussion

The $^{40}Ar/^{39}Ar$ step-heating data are shown in Figure 5 and the analytical results are given in Table 1. The jarosites were step-heated in 4-9 increments and overall yielded fairly flat age spectra (Fig. 5). Sample CJ96-124 from the Copiapo Mine yielded a plateau segment for nearly 85% of the age spectrum and has a corresponding plateau age of 4.68 ± 0.13 Ma (Fig. 5). CJ96-125, also from the

Copiapo Mine, has an age spectrum with an overall age gradient ranging from ~4.3 to ~63 Ma (Table 1; Fig. 5a). However, the first 4 heating steps are nearly concordant and provide a calculated weighted mean age of 4.72 ± 0.28 Ma. This is the preferred age for CJ96-125 despite the fact the age spectrum does not define a rigorous plateau as defined above. The age spectrum for WGND-42 from the Schneider Claim has relatively low resolution (4 steps) due to unexpected laboratory degassing a very low temperatures (Table 1; Fig. 5b). A plateau age of 3.25 ± 0.29 Ma is defined by the initial three heating steps, which contain ~93% of the total ^{39}Ar (Fig. 5b). Most of the heating steps for all of the jarosites have K/Ca values (determined for Ca-derived ^{37}Ar and K-derived ^{39}Ar) between 20 to 200. Additionally, several heating steps did not have detectable ^{37}Ar and thus have infinitely high apparent K/Ca ratios that are left blank on the K/Ca plots (Fig. 5). Considering the relatively young apparent ages of the jarosites, the radiogenic yields are quite high and attain values of up to 80% (Table 1; Fig. 5). This, coupled with the high potassium content, yield total 2σ uncertainties on the order of 3–9% and demonstrate the potential for hypogene jarosite to be a useful geochronometer.

Very little is known about the argon systematics of jarosite. Vasconcelos et al. (1994) published a few supergene jarosite ^{40}Ar/^{39}Ar results for Goldfield, Nevada, and Syama, West Africa. Their findings indicated that low-temperature diffusive radiogenic argon loss, ^{39}Ar recoil and excess argon were not significant problems for dating jarosite. These findings are apparently corroborated by the relatively noncomplex age spectra obtained for the hypogene jarosites reported here. It is noted however, that all of the age spectra (Fig. 5) have high-temperature release steps that are significantly older than the plateau ages. This is especially apparent for CJ96-125, which has a fusion step with an apparent age of ca. 62.5 Ma. Recently, Polyak et al. (1998) report similar age gradients in alunite-age spectra from samples collected in and near caves at Carlsbad Caverns, NM. They convincingly demonstrated that the age gradients, and anomalously old apparent ages, were caused by incomplete supergene alunite replacement of K-bearing Paleozoic clays. An inherited clay component does not appear to be a plausible mechanism to explain the age spectrum apparent age gradients for these hypogene jarosites due to the lack of any K-bearing clay source in the immediate vicinity and the implausibility that a clay would be entrained within the precipitating hydrothermal fluid. Excess ^{40}Ar does not appear to be the cause of the age gradients especially because the measured ages for CJ96-125 (Fig. 5a) climb from ~6 to 63 Ma over the final 40% of the age spectrum despite an essentially constant radiogenic yield. Recoil of ^{39}Ar out of the sample, or redistribution within the sample, is a mechanism often invoked to explain complexities in ^{40}Ar/^{39}Ar age spectra (e.g., Huneke and Smith, 1976; Foland et al., 1984; Lo and Onstott, 1989; Smith et al. 1993). The reaction that converts ^{39}K to ^{39}Ar during neutron irradiation in the reactor involves ~200 KeV of recoil energy that is enough to displace the ^{39}Ar atom approximately 0.1 μm (Turner and Cadogen, 1974). For ultra-fine-grained samples or poorly crystalline material (e.g., glauconite), the recoil energy can be sufficient to eject ^{39}Ar out of the sample, which ultimately results in an apparent age that is too old. Alternatively, mixed phases can yield complex age spectra due to the recoil of ^{39}Ar out of high-K phases and subsequent implantation into low-K phases. Interestingly, the sample with the most severe age gradient is CJ96-125, which is also the sample of natrojarosite, thereby creating a situation with two phases of vastly different K contents. However, even though the potential for ^{39}Ar exchange from the jarosite to the natrojarosite could complicate the age spectrum, it is unclear how this exchange could result in the simple age gradient observed in CJ96-125 (Fig. 5a). Thus, at this stage we are left to ponder the meaning of jarosite-age spectra complexities, but suggest that the minor complexities for these samples do not compromise the interpretation that the apparent plateau and preferred ages are equivalent to the time when the jarosite was precipitated. Therefore, we suggest that the jarosite deposit at Copiapo Mine is 4.69 ± 0.12 Ma based on the combined weighted mean age of the two reported ages for CJ96-124 and CJ96-125. Additionally, the jarosite from Schneider No. 7 claim dates the deposits to be 3.25 ± 0.29 Ma as determined from sample WGNP-42.

These ages compare favorably with the inferred ages at other barite-fluorite deposits in southern New Mexico. The mineralization at Tonuco Mountain, northwest of the study is inferred to be late Miocene-Pliocene (Seager et al., 1971). The age range of jarosite mineralization at Hansonburg was reported by Lueth and Heizler (1997) between 7 and 5.6 Ma. Recently ^{40}Ar/^{39}Ar ages of jarosite has been determined from the Bishop Cap Hills (Bluestar Mine), immediately north of the study area. Preliminary age dates of 5.4–5.10 Ma resulted. Formal documentation of the age dates in the Bishop Cap Hills and other deposits in the Rio Grande rift is still in preparation.

TECTONIC IMPLICATIONS

The Franklin and Organ Mountains of west Texas and southern New Mexico stand in geomorphic disequilibrium with their surroundings, which suggests a relatively young age of uplift. The area lies near the central portion of the Rio Grande rift, which began about 30 Ma (Chapin and Seager, 1975). Traditional thinking required gradual but episodic uplift over the last 30 Ma. Direct evidence to determine the age of uplift or relative rates of uplift in the Franklin-Organ Mountains has not been reported other than the work of Bachman and Mehnert (1978). Recently, Kelley, and Chapin (1997) reported cooling ages utilizing apatite fission-track-length studies from the Organ Mountains. They reported an episode of denudation between 14 and 17 Ma for the central portion of the range. Mack et al. (1993) and Seager and Mack (1995) reported on major Pliocene–Pleistocene normal faulting in an area north of the study area. They documented a total stratigraphic separation of 564 m (maximum) and a relative age of most recent motion at approximately 0.4 Ma associated with a 9 m movement on the fault.

The Copiapo jarosite deposit in Webb Gap is hosted by a currently shallow normal fault. The deposit contains abundant oblique-slip slickensides and drag folds recording post-mineralization fault motions. Provided that the ^{40}Ar/^{39}Ar apparent ages for the jarosites record the time of mineralization within the Copiapo fault, and because mineralization is concluded to be derived from basinal brines based on geochemical constraints, we suggest that the jarosite ages represent basinal dewatering times. We speculate that basin dewatering would be more likely along faults acting as block boundary faults, as it is commonly observed that faults provide ready conduits for fluid migration. Steeply dipping faults are the most common conduits for other barite-fluorite-galena deposits along the rift. Accordingly, the 4.7 Ma age of jarosite records a period when the Copiapo fault was acting as a boundary fault. Subsequently, only minor movements have occurred after it no longer served as an important extensional fault on the western margin of the Hueco Bolson. The 3.25 Ma age at the Schneider deposit potentially records the age of another boundary fault bordering the western edge of the basin. If the mineralization records the age of most significant fault activity, i.e., it served as a block boundary fault on the west side of the Hueco Bolson, significant tectonic activity had to have occurred during the last 5 Ma. That activity would have been responsible for the rotation of the Copiapo fault to shallower angles and produced the subsequent

slickensides and drag folding in the ores.

If we consider a depth of burial at the time of mineralization to be approximately 762 m based on the burial estimates used by Macer (1978) for fluorite deposits in the Organ Mountains, we calculate an estimated uplift rate of 152 m/Ma over the last 5 Ma. This compares favorably to similar estimates derived from the work of Seager and Mack (1995) for the Jornada Draw fault north of the study area. They estimate a maximum displacement of 564 m since the initation of the fault at approximately 2–3 Ma prior to intrusion of the basalt of Black Mountain into the fault at 2.1(?) Ma. Utilizing these constraints, we approximate uplift rates on the fault ranging between 110 to 138 m/Ma on the Jornada Draw fault for the age estimates presented by Seager and Mack (1995).

ACKNOWLEDGMENTS

We acknowledge the assistance of Richard Esser of the New Mexico Geochronological Research Laboratory for help in the $^{40}Ar/^{39}Ar$ dating of jarosite. We also thank Chris McKee for providing assistance in the NMBMMR X-ray facility. This work is supported by the New Mexico Bureau of Mines and Mineral Resources, Charles E. Chapin, Director and State Geologist. Critical and constructive reviews of the manuscript were provided by Andrew Campbell (NMT), Shari Kelley (NMBMMR and NMT), and Jeffrey Hanor (LSU).

REFERENCES

Alpers, C. N., Nordstrom, D. K. and Ball, J. W., 1989, Solubility of jarosite solid solutions precipitated from acid mine waters, Iron Mountains, California, USA: Sciences Geologiques Bulletin, v. 42, p. 281–298.

Bachman, G.O. and Mehnert, H. H., 1978, New K-Ar dates and late Pliocene to Holocene geomorphic history of the Rio Grande region, New Mexico: Geological Society of America Bulletin, v. 89, p. 283–292.

Berliner, M. H., 1949, The Copiapo Jarosite mine, north Franklin Mountains mining district, Doña Ana County, New Mexico: U.S. Bureau of Mines, Examination Report, 7 p.

Berzina, A. P., Kuxnetosova, I. K. and Sotnikov, V. I., 1966, Hypogene jarosite: Geol. Geofiz., v. 8, p. 112–114 (cited in Chemical Abstracts, v. 66, p. 5457).

Chapin, C. E. and Seager, W. R., 1975, Evolution of the Rio Grande rift in the Socorro and Las Cruces areas: New Mexico Geological Society, Guidebook 26, p. 297–321.

Deino, A. and Potts, R., 1990, Single-crystal $^{40}Ar/^{39}Ar$ dating of the Olorgesailie Formation, Southern Kenya Rift: Journal Geophysical Research, v. 95, p. 8453–8470.

Dunham, K. C., 1935, The geology of the Organ Mountains: New Mexico Bureau of Mines and Mineral Resources, Bulletin 11, 270 p.

Fleck, R. J., Sutter, J. F. and Elliot, D. H., 1977, Interpretation of discordant $^{40}Ar/^{39}Ar$ age spectra of Mesozoic tholeiites from Antarctica: Geochemica et Cosmochimica Acta, v. 41, p. 15–32.

Foland, K. A., Linder, J. S., Laskowski, T. E., and Grant, N. K., 1984, $^{40}Ar/^{39}Ar$ dating of glauconites: Measured ^{39}Ar recoil loss from well-crystallized specimens: Isotope Geoscience, v. 2, p. 241–264.

Goodell, P. C., Lueth, V. W. and Heizler, M. T., 1997, $^{40}Ar/^{39}Ar$ age of Rio Grande rift tectonism in the north Franklin Mountains, west Texas and southern New Mexico: Geological Society of America, Abstracts and Programs, v. 29, no. 2, p. 11.

Harbour, R. L., 1972, Geology of the northern Franklin Mountains, Texas and New Mexico: U.S. Geological Survey, Bulletin 1298, 129 p.

Hill, C. A., 1995, Sulfur redox reactions, native sulfur, Mississippi Valley-type deposits and sulfuric acid karst, Delaware Basin, New Mexico and Texas: Environmental Geology, v. 25, p. 16–23.

Huneke, J. C. and Smith, S. P., 1976. The realities of recoil: 39Ar recoil out of small grains and anomalous patterns in ^{39}Ar-^{40}Ar dating: Geochimica et Cosmochimica Acta, Supplement 7 (Proceedings of the Seventh Lunar Science Confernce), p. 1987–2008.

John, D. A., Nash, J. T., Clark, C. W. and Wulftange, W. H., 1991, Geology, hydrothermal alteration, and mineralization at the Paradise Peak gold-silver-mercury deposit, Nye County, Nevada; *in* Proceedings of the Great Basin Symposium, Geological Society of Nevada, p. 1020–1050.

Keith, W. J., Calk, L. and Ashley, R. P., 1979, Crystals of coexisting alunite and jarosite, Goldfield, Nevada: U.S. Geological Survey, Shorter Contributions to Mineralogy and Petrology, C1–C5.

Lo, C.-H. and Onstott, T. C., 1989, ^{39}Ar recoil artifacts in chloritized biotite: Geochimica et Cosmochimica Acta, v. 53, p. 2697–2711.

Kelley, S. A. and Chapin, C. E., 1997, Cooling histories of mountain ranges in the southern Rio Grande rift based on apatite fission-track analysis-a reconnaissance survey: New Mexico Geology, v. 19, p. 1–14.

Kelley, S. A. and Matheny, J. P., 1983, Geology of the Anthony quadrangle, Doña Ana County, New Mexico: New Mexico Bureau of Mines and Mineral Resources, Geologic Map 54, scale 1:24,000.

Long, D. T., Fegan, N. E., Lyons, W. B., Hines, M. E., Macumber, P. G. and Giblin, A. M., 1992, Geochemistry of acid brines: Lake Tyrell, Victoria, Australia: Chemical Geology, v. 96, p. 33–52.

Lueth, V. W. and Goodell, P. C., 1996, A remarkable deposit of jarosite: The product of rift basin dewatering: Geological Society of America, Abstracts and Programs, v. 28, no. 7, p. A-210.

Lueth, V. W. and Heizler, M. T., 1997, $^{40}Ar/^{39}Ar$ age and origin of jarosite mineralization at the Hansonburg district, New Mexico: New Mexico Geology, v. 19, p. 51.

Macer, R. J., 1978, Fluid inclusion studies of fluorite around the Organ Cauldron, Doña Ana County, New Mexico [M.S. thesis]: El Paso, University of Texas at El Paso, 107 p.

Mack, G. H., Salyards, S. L. and James, W. C., 1993, Magnetostratigraphy of the Plio–Pleistocene Camp Rice and Palomas Formations in the Rio Grande rift of southern New Mexico: American Journal of Science, v. 293, p. 49–77.

Macumber, P. G., 1992, Hydrological processes in the Tyrell Basin, southeast Australia: Chemical Geology, v. 96, p. 1–19.

McLemore, V. T., Sutphin, D. M., Hack, D. R. and Pease, T. C., 1996, Mining history and mineral resources of the Mimbres Resource Area, Doña Ana, Luna, Hidalgo, and Grant Counties, New Mexico: New Mexico Bureau of Mines and Mineral Resources, Open-file Report 424, 251 p.

Michel, F. A. and Van Everdingen, R. O., 1987, Formation of a jarosite deposit on Cretaceous shales in the Fort Norman area, Northwest Territories: Canadian Mineralogist, v. 25, p. 221–226.

Polyak, V. J. and G¸ven, N., 1996, Alunite, natroalunite, and hydrated halloysite in Carlsbad Cavern and Lechuguilla Cave, New Mexico: Clays and Clay Minerals, v. 44, p. 843–850.

Polyak, V. J., McIntosh, W. C., Guven, N., and Provencio, P., 1998, Age and origin of Carlsbad Cavern and related caves from $^{40}Ar/^{39}Ar$ dating of alunite: Science, v. 279, p. 1919–1922.

Putnam, B. R., Norman, D. I. and Smith, R. W., 1993, Mississippi Valley-type lead-fluorite-barite deposits of the Hansonburg mining district: New Mexico Geological Society, Guidebook 34, p. 253–259.

Rye, R. O. and Alpers, C. N., 1997, The stable isotope geochemistry of jarosite: U.S. Geological Survey, Open-file Report 97-88, 28 p.

Samson, S. D. and Alexander, E. C., Jr., 1987, Calibration of the interlaboratory $^{40}Ar/^{39}Ar$ dating standard, Mmhb-1: Chemical Geology and Isotopic Geoscience, v. 66, p. 27–34.

Seager, W. R. and Mack, G. H., 1995, Jornada Draw fault: A major Pliocene–Pleistocene normal fault in the southern Jornada del Muerto: New Mexico Geology, v. 17, p. 37–43.

Seager, W. R., Hawley, J. W. and Clemons, R. E., 1971, Geology of San Diego Mountain Area, Doña Ana County, New Mexico: New Mexico Bureau of Mines and Mineral Resources, Bulletin 97, 38 p.

Smith, P. E., Evensen, N. M. and York, D., 1993, First successful $^{40}Ar/^{39}Ar$ dating of glauconies; argon recoil in single grains of cryptocrystalline material: Geology v. 21, p. 41–44.

Steiger, R. H. and Jager, E., 1977, Subcommission on geochronology: Convention on the use of decay constants in geo- and cosmochronology: Earth and Planetary Science Letters, v. 36, p. 359–362.

Stoffregen, R. E., 1993, Stability relations of jarosite to natrojarosite at 150–250°C: Geochimica et Cosmochimica Acta, v. 57, p. 2417–2429.

Turner, G. and Cadogan, P. H., 1974, Possible effects of ^{39}Ar recoil in $^{40}Ar^{39}Ar$ dating: Proceedings of the 5th Lunar Planetary Conference, Geochimica et Cosmochimica Acta, supplement 5, p. 1601–1615.

Vasconcelos, P. M., Brimhall, G. H., Becker, T. A. and Renne, P. R., 1994, $^{40}Ar/^{39}Ar$ analysis of supergene jarosite and alunite: Implications to the paleoweathering history of the western USA and West Africa:

View looking west of the central part of the Robledo Mountains. High cliffs belong to the Permian Hueco Formation, and bluffs in foreground are late Pleistocene alluvial-fan sediment dissected during the Holocene. Photograph by Greg Mack.